Materials and Structures/Matériaux et Constructions, Vol. **31**, June 1998, pp 317-324

Microstructure and transport properties of porous building materials

Daniel A. Quenard[1], *Ke Xu*[1], *Hartwig M. Künzel*[2], *Dale P. Bentz*[3] *and Nicos S. Martys*[3]

(1) Centre Scientifique et Technique du Batiment, Service Matériaux, 24 Rue Joseph Fourier, F-38400 Saint-Martin d'Hères, France

(2) Fraunhofer-Institut für Bauphysik, IBP Postfach 11 52, D-83601 Holzkirchen, Germany

(3) National Institute of Standards and Technology, Building Materials Division, Building and Fire Research Laboratory, U.S. Department of Commerce, Gaithersburg, MD 20899, U.S.A.

Paper received: February 13, 1997; Paper accepted: April 3, 1997

ABSTRACT

To successfully predict the performance of building materials exposed to a degradative environment, transport properties must be either measured or estimated. The development of relationships between microstructure and transport properties for these materials should allow accurate prediction of the latter and an increased understanding of how microstructure influences transport. Here, two microstructural characterization techniques, mercury intrusion porosimetry and scanning electron microscopy, are combined with computer modelling techniques to compute the vapor diffusivity and air permeability of three building materials commonly exposed in building facades, two types of brick and a natural sandstone. In general, the computed values compare favorably to those measured experimentally, thus demonstrating the capability of employing microstructural characterization to predict transport properties.

RÉSUMÉ

Pour obtenir une prédiction fiable des performances des matériaux de construction exposés à un environnement agressif, leurs propriétés de transport doivent être soit mesurées soit estimées. Le développement de relations entre la microstructure et les propriétés de transport devrait permettre une prédiction exacte de ces dernières et une meilleure compréhension de l'influence de la microstructure sur le transfert. Dans cet article, deux techniques de caractérisation de la microstructure (porosimétrie au mercure et microscopie électronique à balayage) sont combinées avec des techniques de simulation par ordinateur pour calculer la diffusivité à la vapeur d'eau et la perméabilité à l'air de trois matériaux de construction traditionnellement utilisés en facades : deux types de brique et un grès naturel. En général, les valeurs calculées sont proches de celles mesurées expérimentalement. Ces résultats démontrent les possibilités des outils de caractérisation de la structure pour prédire les propriétés de transport.

1. INTRODUCTION

The moisture behavior of exposed building elements has a predominant influence on their durability because water is often a major reason for damage or decay. Therefore, the vapor and liquid transport properties of porous surface materials are of great practical importance. However, while the vapor diffusivity of a dry material is rather easy to measure, the determination of the more important water vapor diffusivity under partially-saturated conditions is more complex, since it depends upon the local water content and, to a certain extent, upon the boundary conditions [1]. For this reason, it would be advantageous if the transport properties of porous materials could be derived from their microstructures. The purpose of this paper is to compare the measured transport properties of three common building materials to those computed based on microstructural information consisting of either pore-size distributions, as measured by mercury intrusion porosimetry, or two-dimensional scanning electron microscopy images.

2. EXPERIMENTAL INVESTIGATION

For this investigation, three building materials were used which are commonly exposed in building facades. Two bricks were examined: a lime-silica brick formed by high pressure steam curing of a mixture of lime and silica, and a clinker brick which is a hard-burned clay brick. Both

Editorial note:
Mr. Daniel Quenard is a RILEM Senior Member and a member of TC 123-MME on the Use of Microstructural Models and Expert systems for Cementitious Materials. He and Mr. K. Xu work at the CSTB (Centre Scientifique et Technique du Bâtiment), France, a RILEM Titular Member. Mr. Dale P. Bentz is a RILEM Senior Member and participates in the work of TC 159-ETC (Engineering of the Interfacial Transition Zone in Cementitious Composites). He and Mr. Nicos Martys work at the National Institute of Standards and Technology (NIST), USA, a RILEM Titular Member.

1359-5997/98

types of masonry units are used in the rain screens of cavity walls. The third material, Baumberger Sandstone, is a natural lime sandstone found in historic buildings and used as facade elements in their modern reproductions. In order to determine the open porosity of these materials, the true density was measured with the aid of a helium pycnometer and then compared to the bulk density. To obtain the transport properties and the necessary microstructural information, the following tests were carried out.

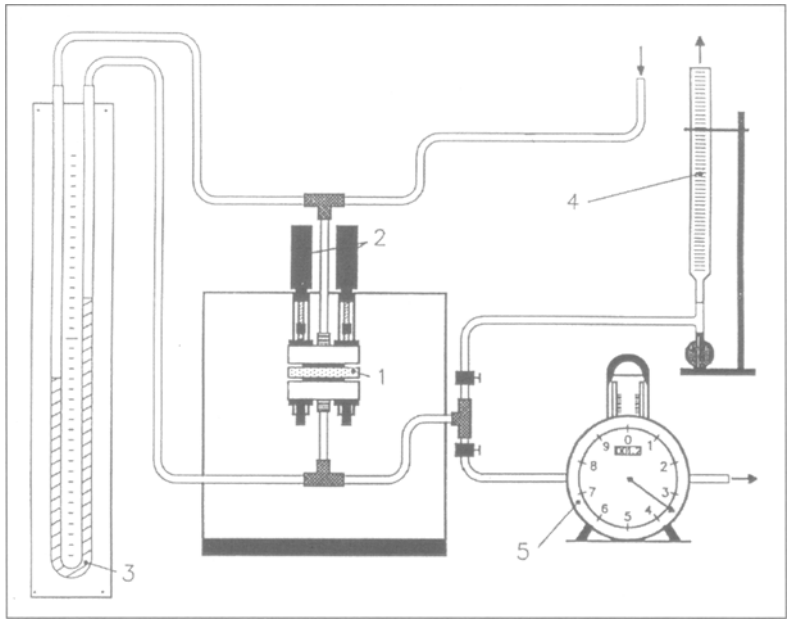

Fig. 1 – Sketch of the device for the air permeability tests – 1: specimen; 2: screw clamb; 3: U-tube manometer; 4: bubble flowmeter; 5: alternative flowmeter.

2.1 Measurement of vapor diffusivity

The vapor diffusivity was measured by means of a cup test according to the DIN standard 52 615 [2]. For this test, samples of at least 100 cm^2 in area were sealed to a cup containing silica gel (3% RH) and then exposed to constant climatic conditions of 23 °C and 50% RH. The test was completed when the rate of mass increase of the cups was linear, *i.e.* the material sample had reached a steady state in terms of moisture transport. The vapor diffusivity was then calculated using the following equation:

$$D_p = \frac{G\, d_s}{A_s\ \Delta c} \qquad (1)$$

where:
D_p = vapor diffusivity of porous material (m^2/h)
G = constant rate of weight increase of test cup (g/h)
d_s = sample thickness (m)
A_s = sample area (m^2)
Δc = vapor concentration difference between inside and outside of test cup (g/m^3).

2.2 Measurement of water absorption coefficient

The water absorption of each material was measured by placing one surface of the dried samples from the cup test in contact with liquid water, leaving the other surface in contact with laboratory air. Since the samples were sealed on all sides, water absorption can only take place through the lower surface of the sample. The samples were weighed at regular time intervals until the water reached the upper surface. The mass increase per unit area (M/A_s) was plotted vs. the square root of time which resulted in a straight line, whose slope yielded the water absorption coefficient:

$$B = \frac{M}{A_s\sqrt{t}} \qquad (2)$$

where:
B = water absorption coefficient ($kg/m^2\sqrt{h}$)
M = water uptake since start of test (kg)
A_s = sample area (m^2)
t = time elapsed since start of test (h).

2.3 Measurement of air permeability

The measurement of air permeability was carried out on the same samples as the other two tests, after they had been dried again. To perform the measurement, the samples were introduced into the test device shown in Fig. 1, where they were tightly clamped between the rubber seals of two flanges. Then, the air flow through the sample was measured for different pressure drops (10 to 200 mbar) either by a rotating gas flowmeter or by a bubble flowmeter, depending on the rate of air flow through the sample. As long as the air fluxes for different pressure drops lie on a straight line when plotted against the pressure gradient, the flow is considered to be laminar, and the air permeability can be determined from the equation:

$$K_D = \frac{Q\ \mu\ d_s}{A_s\ \Delta\ P_L} \qquad (3)$$

where:
K_D = air permeability (m^2)
Q = air flux (m^3/s)
μ = air viscosity (kg/m/s)
d_s = sample thickness (m)
A_s = sample area (m^2)
ΔP_L = air pressure difference (Pa).

2.4 Mercury intrusion porosimetry (MIP)

The MIP measurements were carried out with a low pressure and a high pressure (max. 200 MPa) porosimeter from Carlo Erba. The volumes of the test samples varied between 2 and 4 cm^3, and mainly consisted of two pieces. Prior to the test, the samples were dried at 40 °C with dry air (dew point of below -40 °C). The evaluation of the tests was conducted assuming cylindrical pores, a contact angle of 141.3°, and a mercury surface tension of

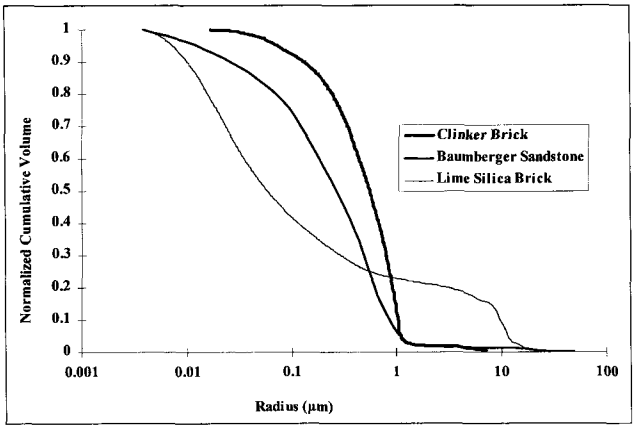

Fig. 2 – Mercury Intrusion Porosimetry: Clinker Brick - Lime Silica Brick - Baumberger Sandstone.

0.48 N/m. The resulting cumulative pore size distributions for each of the three materials are shown in Fig. 2.

2.5 Scanning electron microscopy (SEM)

The examination by microscopy of polished specimens of porous materials is facilitated if the pores are filled with a hard material such as an epoxy resin. The resin serves to stabilize the microstructure and provides support to prevent damage during polishing and microcracking during the SEM investigation. The resin, due to its low average atomic number, may also improve the identification of pores using scanning electron microscopy with backscattered electron imaging (BEI).

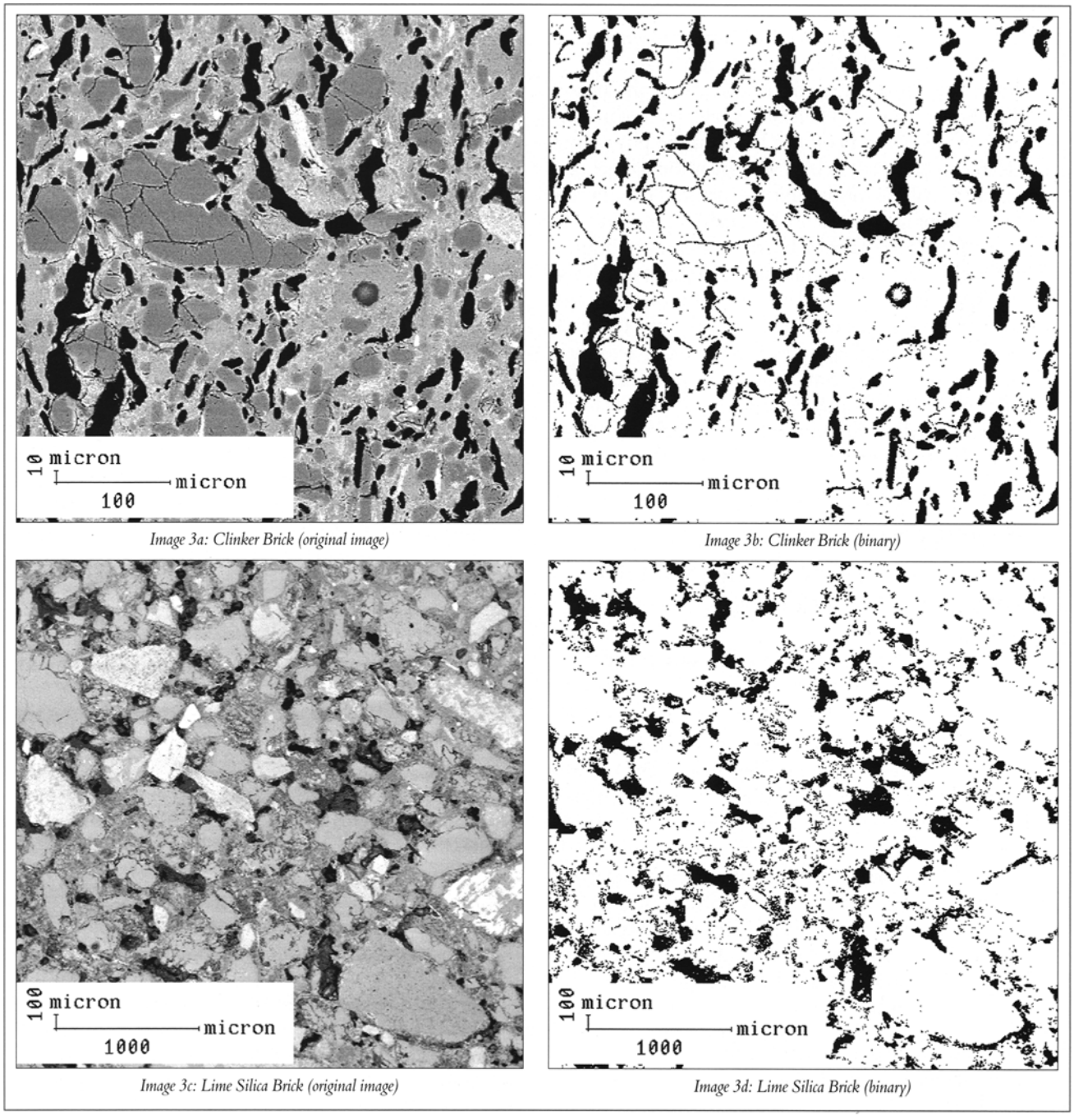

Image 3a: Clinker Brick (original image)

Image 3b: Clinker Brick (binary)

Image 3c: Lime Silica Brick (original image)

Image 3d: Lime Silica Brick (binary)

Fig. 3 – Original and binarized images of the two bricks. Porosity in black.

Table 1 – Characteristics of the images		
	Clinker Brick	Lime Silica Brick
Image Size (pixel)	512 × 512	512 × 512
SEM Magnification	200	25
Micron/Pixel Ratio	1 pixel = .867 μm	1 pixel = 6.94 μm
Porosity (%)	19	16

The procedure used to fill the pores with the epoxy resin is described in [3]. The sample is a thin slice with dimensions 10 mm by 10 mm by 2 mm. The resin layer on the face of the specimen is removed by grinding and afterwards the surface is polished and cleaned. This process can be repeated as often as necessary. The impregnated polished samples are then sputter-coated with a thin carbon layer under vacuum and examined with an SEM in the backscattered electron mode.

The size of the analyzed area depends on the phases which are being analyzed. Generally, a high level of magnification provides a good contrast between the phases, but the investigated area is often smaller than the elementary representative volume of the microstructure. The thresholding is a major step in the image analysis procedure. In our case, since the contrast between phases is high, a method based on the local minima in the grey-level histogram is sufficiently effective [4]. The original and processed binary images obtained from the clinker brick and the lime-silica brick are presented in Fig. 3 and their main characteristics are detailed in Table 1. A fraction of the pores in the Baumberger Sandstone was too small and their overall size distribution too broad to be reliably distinguished in a single image using the SEM technique.

3. MICROSTRUCTURE MODELLING AND COMPUTATION OF TRANSPORT PROPERTIES

3.1 Reconstruction of a 3-D microstructural image

Starting with the binary 2-D (two-dimensional) images of the clinker and lime-silica bricks, 3-D representations were reconstructed using the computational techniques outlined in [5]. Basically, the autocorrelation function of the original 2-D image is used to filter a 3-D image of random noise, which is subsequently binarized and modified using a surface curvature algorithm [6]. This results in the creation of a 3-D microstructural image with the same porosity and specific surface (hydraulic radius) as the original 2-D image.

For an MxN image, the two-point correlation function for the porosity, S(x,y), is determined by:

$$S(x,\,y)=\sum_{i=1}^{M-x}\sum_{j=1}^{N-y}\frac{I(i,\,j)\cdot I(i+x,\,j+y)}{(M-x)(N-y)}$$

where I(x,y) is one if the pixel at location (x,y) is labelled as porosity and zero otherwise. These values are then converted to S(r) for distances r in pixels by [7]:

$$S(r)=\frac{1}{2r+1}\sum_{l=0}^{2r}S\left(r,\frac{\pi l}{4r}\right)$$

where for angles θ, S(r, θ) = S(r.cosθ, r.sinθ) is obtained by bilinear interpolation from the values of S(x,y).

The measured two-point correlation function is used to filter a 3-D image, N(x,y), consisting of random noise following a normal distribution, generated using the Box-Muller method [8]. The filter employed, F(x,y,z), is the normalized version of the two-point correlation function obtained by:

$$F(x,y,z)=\frac{S\left(r=\sqrt{(x^2+y^2+z^2)}\right)-S(0)^2}{S(0)-S(0)^2}$$

The resultant image is then calculated as:

$$R(x,y,z)=\sum_{i=0}^{30}\sum_{j=0}^{30}\sum_{k=0}^{30}N(x+i,\;y+j,\;z+k)\cdot F(i,j,k)$$

After the filtering is performed, a threshold value is selected and applied such that the appropriate porosity fraction will be present in the binarized 3-D image. Finally, to better match the specific surface of the original 2-D image, this 3-D image is rearranged by interchanging porosity pixels at high curvature locations with solid pixels located at low curvature sites [6]. The curvature is simply defined as being proportional to the fraction of porosity pixels in some local neighborhood (*e.g.* a 3*3*3 cube or sphere) around the pixel being evaluated. This algorithm is performed iteratively until the correct hydraulic radius as been attained in the 3-D system.

In the case of the clinker brick, the 3-D microstructure was reconstructed with porosities of both 19% and 20%, to match both the original 2-D SEM image and the measured open porosity based on the bulk and true densities. Fig. 4 shows a portion of the reconstructed 3-D clinker brick microstructure. Although discontinuous in 2-D, the pore systems of the reconstructed brick images are continuous in three dimensions, as verified computationally using a burning algorithm [9].

3.2 Computation of transport properties using digital images

The reconstructed 3-D microstructures were used as input into two computational programs to compute both their relative diffusivity (formation factor) and their permeability.

The relative diffusivity (the diffusivity of a species in the porous medium relative to its diffusivity in bulk liquid or gas of the same composition as that contained in the pores) is computed based on an electrical analogy solution of Laplace's equation using a conjugate gradient technique [10].

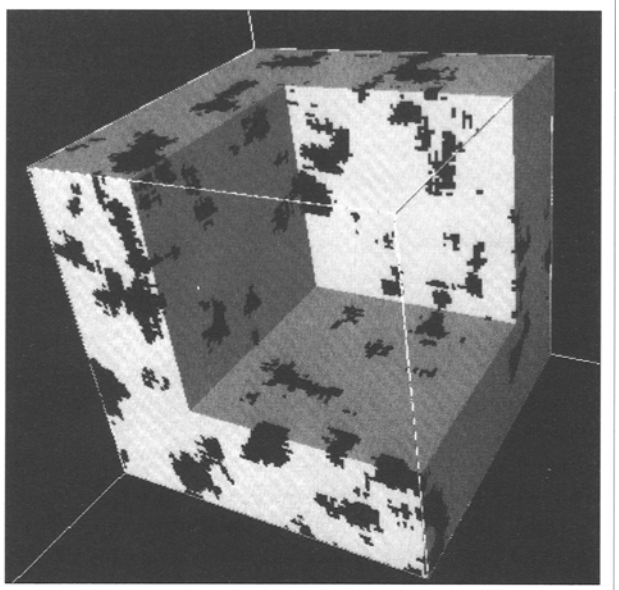

Image 4a: Clinker Brick

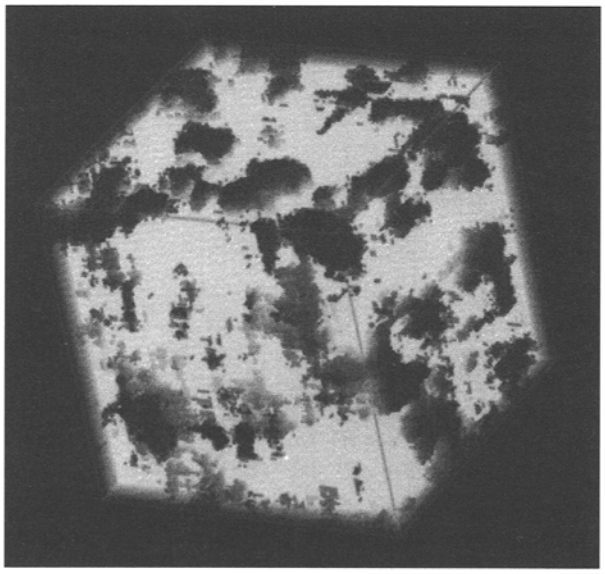

Image 4b: Lime Silica Brick

Fig. 4 – 3-D reconstructed images.

According to the Nernst-Einstein relation, the computed relative conductivity is equivalent to the desired relative diffusivity. For the lime-silica brick, since the SEM/reconstruction technique only generates the macro-porosity (pores larger than about 10 μm), the solids (normally assigned a relative conductivity of 0) were assigned a relative conductivity value of 0.005, the value computed for a 3-D image of the lime-silica brick with a porosity of 16%. Here, we are assuming that the tortuousity of the porosity below the resolution threshold of the SEM is identical to that of the resolvable pores. Thus, the total open porosity fraction of the 3-D system would be 0.16 + (1 - 0.16)*0.16 = 0.294, very close to the value of 0.30 measured experimentally. This multi-scale approach to computing the diffusivity of porous materials has been successfully demonstrated for cement-based materials [11]. The macro-pores in both systems were assigned a relative conductivity of 1. The relative diffusivities reported in the results section are the averages of the values determined for a voltage drop applied in each of the three principal directions. A value of 0.0922 m^2/h [12] was used as the diffusivity of water vapor in air to convert the relative diffusivity values to absolute ones for comparison with experimental data.

To determine the permeability of the 3-D brick images, Stokes equation for slow incompressible flow was solved using a finite difference scheme along with non-centered difference equations [13, 14]. A pressure gradient is applied across the microstructure and the velocities are determined at all nodes (pixels). The permeability is then calculated by volume averaging these local velocities and applying the Darcy equation. Since, in this case, the permeability is dominated by the largest connected pores, no attempt was made to incorporate the micro-porosity of the lime-silica brick specimens into the computation. Once again, the permeabilities reported in the results are the averages of the permeabilities computed in each of the three principal directions.

3.3 Computation of transport properties using renormalization techniques

The pore sizes of porous building materials may cover several orders of magnitude, generally ranging from nanometers to a few micrometers. Therefore, it is often difficult to relate porosity and transport properties for such materials. A method based on the representation of the pore structure by networks of capillary tubes has been proposed by Daian *et al.* [15].

The basic idea is to sort the pore size distribution (PSD) into several classes and to distribute each class on a network of a different size (Fig. 5). A porous medium with a large PSD will be described as the superposition of n monoscale lattices representative of the various size classes of pores present in the material. Fig. 5 shows an example with 3 classes and a scaling ratio of 2. The mesh size of each lattice is proportional to the corresponding pore size, and the occupation probability of each lattice is

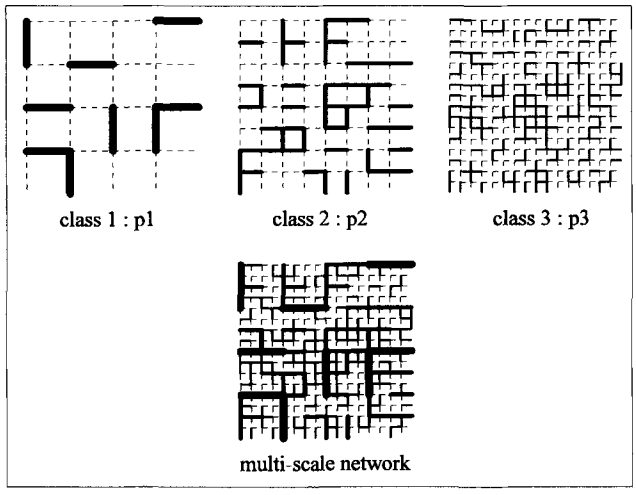

Fig. 5 – 3 monoscale networks with probability p_i and the multi-scale network obtained by superposition.

p_i [15]. The different networks are then superposed by following rules based on renormalization theory; the multi-scale structure obtained by a simple superposition process is also presented in Fig. 5.

This model is applied to correct the PSD obtained from the experimental mercury intrusion porosimetry (MIP) curves [16, 17]. Figs. 6, 7 and 8 show the experimental MIP curves, the points selected for the fitting by the renormalization process, and the corresponding "corrected" curves (the true pore size distribution for the renormalization "3-D tube network" structure without any ink bottle effects) obtained for the three examined materials.

Then, using the "corrected" PSDs, the air permeability and the water vapor diffusivity can be estimated again using a renormalization method [18]. The liquid flow in each capillary tube is approximated by Poiseuille flow and vapor diffusion in air, as described by Fick's law.

4. RESULTS AND DISCUSSION

The experimental results for density, open porosity, vapor diffusivity and air permeability, as well as the water absorption coefficients of the three examined materials, are listed in Table 2, along with the transport coefficients computed using the microstructural models. For the clinker brick, the reported transport coefficients are for the reconstructed microstructure with a porosity of 20%.

In comparing the transport properties of the three materials, it is obvious that both open porosity and pore size are important. Thus, the air permeability of the clinker brick is significantly higher than that of the Baumberger Sandstone, even though the converse is observed for vapor diffusivity. From Fig. 2, this can be attributed to the larger pore sizes present in the finding clinker brick, as permeability is generally proportional to pore size squared, whereas the vapor diffusivity does not depend on the pore size, except for the Knudsen diffusion in smaller pores (pore radius < mean free path of the vapor molecules). For the three materials examined here, the measured air permeabilities (Table 2) rank in the same order as the critical pore sizes measured by MIP (Fig. 2), where the critical pore size corresponds to the (first) inflection point in the MIP cumulative intrusion curve [19].

Both microstructural modelling techniques incorporate information on total porosity and pore size, two of the controlling variables in determining the magnitude of transport in a porous media. The connectivity or tortuosity of the pore space, a third critical parameter, is incorporated somewhat implicitly from the autocorrelation analysis of the 2-D binary image, or from matching the simulated and experimental MIP curves in the renormalization technique.

Table 2 - Physical and transport properties of materials investigated

Material or Transport Property	Lime Silica Brick	Clinker Brick	Baumberger Sandstone
Bulk Density (kg/m^3)	1830	2080	2070
True Density (kg/m^3)	2600	2610	2660
Open Porosity (%)	30	20	22
Experimental Air Permeability (μm^2)	0.039	0.006	0.001
Computed Air Permeability-Reconstruction (μm^2)	0.057	0.0046	not determined
Computed Air Permeability-Renormalization (μm^2)	0.017 (1) [a] 0.018 (2) 0.042 (3)	0.0015 (1) 0.0099 (2)	0.0012 (1) 0.0064 (2) 0.0108 (3)
Water Absorption Coefficient ($kg/m^2h^{0.5}$)	9	3	9
Experimental Vapor Diffusivity (m^2/h)	0.004	0.002	0.005
Computed Vapor Diffusivity-Reconstruction (m^2/h)	.002	.0015	not determined
Computed Vapor Diffusivity-Renormalization (m^2/h)	0.00050 (1) 0.00027 (2)	0.00060 (1) 0.00076 (2)	0.00068 (1) 0.00044 (2) 0.00044 (3)

[a] : *The reference number 1, 2 or 3 indicates the MIP curves in Figs. 6, 7 and 8 used to compute the transport coefficients.*

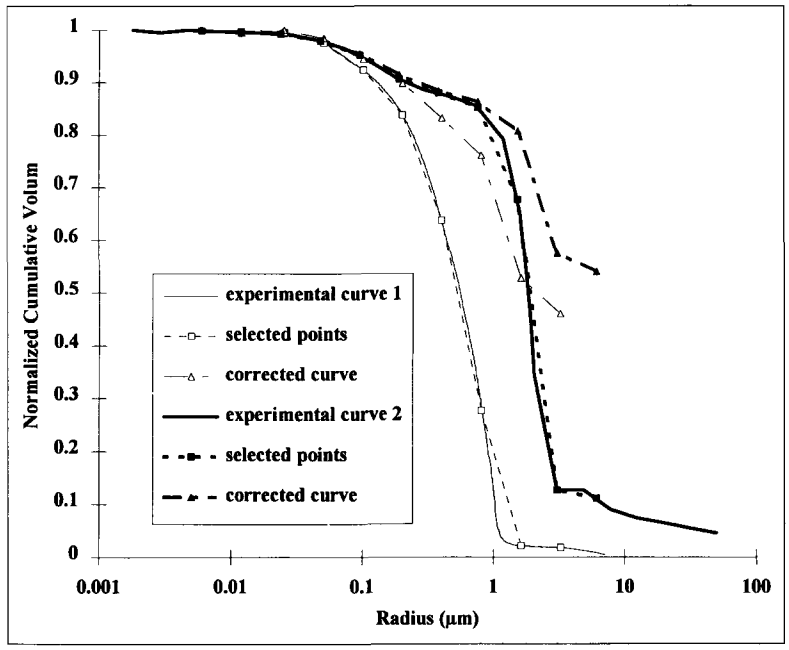

Fig. 6 - Mercury Intrusion Porosimetry: Clinker Brick.

The two modelling techniques both appear to be valid means for computing the air permeabilities of these building materials from microstructural measurements. The reconstruction technique and subsequent image-based computations provided permeabilities and diffusivities both within a factor of 2 of those measured experimentally. Likewise, the renormalization technique resulted in average permeabilities generally close to the experimental values. However, concerning diffusivities,

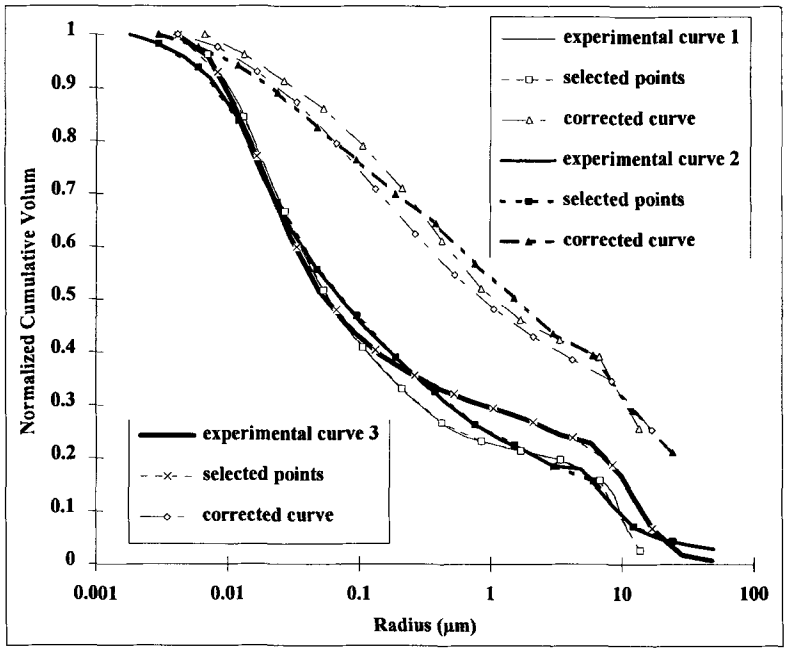

Fig. 7 – Mercury Intrusion Porosimetry: Lime Silica Brick.

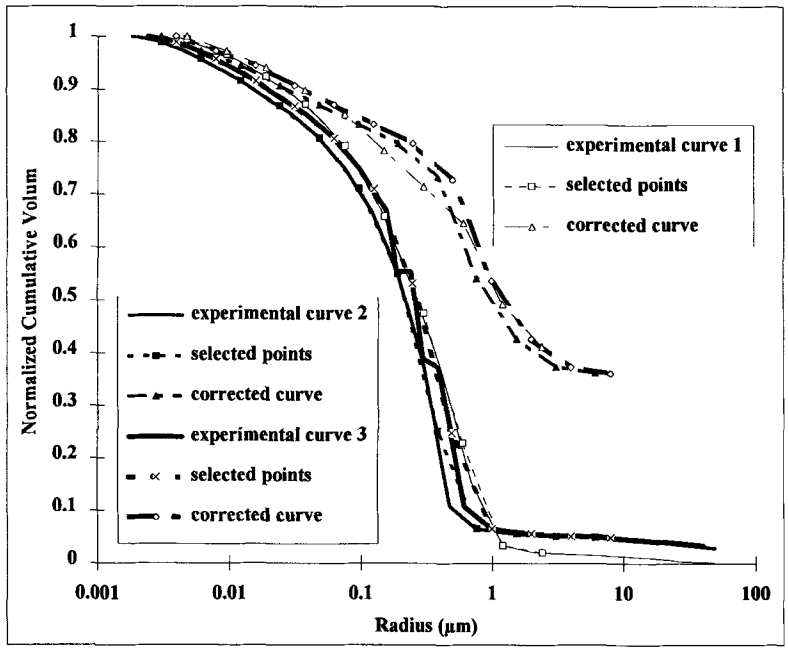

Fig. 8 – Mercury Intrusion Porosimetry: Baumberger Sandstone.

the discrepancies between experimental results and the renormalization model are much higher, around one order of magnitude.

These differences are not yet explained, but may be due to different causes. First, the contributions of the smallest pores (radius below 4 nm, not detected by MIP or SEM investigations) are not considered by both computation techniques. Second, the largest pores (on the order of 50-100 μm according to the micrographs in Fig. 3) are not well taken into account by the renormalization technique (Figs. 6, 7 and 8). Third, the connectivity of the actual microstructures may differ from that of the cubic lattice which underlies the renormalization model.

5. CONCLUSIONS

Characterizing the microstructure of porous building materials using scanning electron microscopy or mercury intrusion porosimetry provides valuable information for use in microstructural models for computing transport properties. In this study, these microstructural models, in conjunction with computations, provided estimates of air permeability which were in good agreement with experimental measurements for three commonly-used building materials.

Concerning vapor diffusivity, the SEM-based modelling technique underestimated the measured coefficient by up to a factor of 2, while the renormalization-based modelling technique resulted in values up to an order of magnitude below those measured experimentally.

ACKNOWLEDGEMENTS

Dale Bentz would like to thank the Centre International des Étudiants et Stagiaires (C.I.E.S.) for a grant which allowed this research to be pursued during a six month stay at the Centre Scientifique et Technique du Bâtiment in France. This study was conducted as part of the European Science Project CT 91-0737, entitled "Characterization of Microstructure as a Tool for Prediction of Moisture Transfer in Porous Media".

REFERENCES

[1] Kiessl, K., Krus, M. and Künzel, H.M., 'Weiterentwickelte Mess- und Rechenansätze zur Feuchtebeurteilung von Bauteilen', *Bauphysik* **15** H.2 (1993) 61-67.

[2] DIN 52 615: Bestimmung der Wasserdampfdurchlässigkeit von Bau- und Dämmstoffen, 1987.

[3] Struble, L., Stutzman, P.E., 'Epoxy impregnation of hardened cement for microstructural characterization', *Journal of Materials Science Letters* **8** (1989) 632-634.

[4] Castleman, K., 'Digital Image Processing' (Prentice-Hall, Inc., Englewood Cliffs, NJ, 1979).

[5] Bentz, D.P. and Martys, N.S., 'Hydraulic radius and transport in reconstructed model three-dimensional porous media', *Transport in Porous Media* **17** (3) (1995) 221-238.

[6] Pimentia, P.J.P., Carter, W.C. and Garboczi, E.J., 'Cellular automaton algorithm for surface mass transport due to curvature gradients: Simulations of sintering', *Computational Materials Science* **1** (1992) 630-37.

[7] Berryman, J. G., 'Measurement of spatial correlation functions using image processing techniques', *Journal of Applied Physics* **57** (7) (1985) 2374-2384.

[8] Law, A.M. and Kelton, W.D., 'Simulation Modeling and Analysis' (Mc Graw-Hill, New York, 1982).
[9] Stauffer, D., 'Introduction to Percolation Theory' (Taylor and Francis, London, 1985).
[10] Garboczi, E.J. and Bentz, D.P., 'Computer simulation of the diffusivity of cement-based materials', *Journal of Materials Science* **27** (1992) 2083-92.
[11] Bentz, D.P., Garboczi, E.J. and Martys, N.S., 'Application of digital-image-based models to microstructure, transport properties, and degradation of cement-based materials', in 'The Modeling of Microstructure and Its Potential for Studying Transport Properties and Durability', Eds. H.M. Jennings *et al.*, (Kluwer Academic Publishers, 1996) 167-186.
[12] Holman, J.P., 'Heat Transfer' (McGraw-Hill, New York, 1981).
[13] Martys, N.S. and Garboczi, E.J., 'Length scales relating the fluid permeability and electrical conductivity in random two-dimensional model porous media', *Phys. Rev. B 46* (1992) 6080-88.
[14] Schwartz, L.M., Martys, N.S., Bentz, D.P., Garboczi, E.J. and Torquato, S., 'Cross property pelations and permeability estimation in model porous media', *Phys. Rev. E* **48** (1993) 4584-91.
[15] Daian, J.F., Xu, K. and Quenard, D., 'Invasion and transport processes in multiscale model structures for porous media', COPS III, IUPAC Symp. on the Characterization of Porous Solids, Marseille, 1993.
[16] Daian, J.F., Xu, K. and Quenard, D., 'Multiscale models: A tool to describe the porosity of cement-based materials and to predict their transport properties', in 'The Modeling of Microstructure and Its Potential for Studying Transport Properties and Durability', Eds. H.M. Jennings *et al.* (Kluwer Academic Publishers, 1996) 107-136.
[17] Xu, K., "Structures multichelles: Modèles pour la Description des Matériaux Poreux et l'Estimation de leurs Propriétés de Transport', Ph.D Thesis, Université Joseph Fourier - Grenoble I, 1995.
[18] King, P.R., 'The use of renormalization for calculating effective permeability', *Transport in Porous Media* **4** (1) (1989) 37-58.
[19] Katz, A.J. and Thompson, A.H., *Journal of Geophysical Research* **92** (B1) (1987) 599 and *Phys. Rev. B* **34** (1986) 8179.